# RECENT RESULTS FROM A MODEL OF THE HALL THRUSTER DISCHARGE

**E. Ahedo, J.M. Gallardo, F.I. Parra, and C. Pérez Trigo**

E.T.S.I. Aeronáuticos, Universidad Politécnica de Madrid, Spain

**IEPC-2003-331**

**Abstract**

The analysis of a model of the axial discharge which included source terms accounting for the effects of the radial plasma-wall interaction was completed recently. Some of the main aspects and results are summarized here together with later parametric investigation on the magnetic strength versus discharge voltage curve.

## 1 Axial model with wall effects

Reference [1] presents the quasi one-dimensional model of the plasma discharge in a stationary plasma thruster with the effects of the lateral plasma-wall interaction. These consist of (i) plasma recombination, (ii) energy losses, and (ii) extra axial diffusion due to secondary/primary electron exchanges (i.e. 'wall collisionality'). The main plasma equations of the model are:

$$\frac{1}{A}\frac{d}{dx}(An_e v_{xi}) = n_e(\nu_i - \nu_w), \tag{1}$$

$$\frac{1}{A}\frac{d}{dx}(Am_i n_e v_{xi}^2) = -en_e\frac{d\phi}{dx} - \frac{dn_eT_i}{dx} + m_i n_e(\nu_i v_{xn} - \nu_w v_{xi}), \tag{2}$$

$$0 = -\frac{d}{dx}n_eT_e + en_e\frac{d\phi}{dx} - m_e n_e v_{xe}\frac{\omega_e^2}{\nu_e}, \tag{3}$$

$$\frac{1}{A}\frac{d}{dx}A\frac{5}{2}T_e n_e\Big(v_{xe} - \frac{\omega_e^2}{\nu_e m_e}\frac{dT_e}{dx}\Big) = e\frac{d\phi}{dx}n_e v_{xe} - \nu_i\alpha_i E_i n_e - \nu_{we}T_e n_e. \tag{4}$$

Here, $E_i$ is the ionization potential, $\alpha_i$ is the ionization cost factor, $\nu_i = n_n\sigma_i\sqrt{8T_e/\pi m_e}$ is the ionization frequency, and

$$\nu_e = \nu_{en} + \nu_{ei} + \nu_{wm} + \alpha_{ano}\omega_e \tag{5}$$

is the effective axial diffusion frequency for electrons (with contributions of electron-neutral and electron-ion collisions, wall 'collisions', and anomalous diffusion generated by fluctuating fields). The source terms for the wall effects are characterized by the plasma recombination frequency,

$$\nu_w = \frac{\tilde{\nu}_w}{h_c}\sqrt{\frac{T_e}{m_i}}, \tag{6}$$

the energy loss frequency,

$$\nu_{we} = \beta_e\nu_w, \qquad \beta_e(\delta_w) \simeq 7.77 + 1.65\,\frac{\delta_w}{1-\delta_w}, \tag{7}$$

and the wall collisionality frequency,

$$\nu_{wm} = \beta_m\nu_w. \qquad \beta_m(\delta_w) \simeq \frac{\delta_w}{1-\delta_w}. \tag{8}$$

Here, $\tilde{\nu}_w$ is a dimensionless parameter, which should be determined by the radial problem, and $\delta_w$ is the effective secondary electron emission(SEE) yield, which follows,

$$\delta_w(T_e) = \begin{cases} \sqrt{T_e/T_1}, & T_e \leq T_e^*, \\ \delta_w^*, & T_e > T_e^*, \end{cases} \tag{9}$$

where the asterisk indicates charge-saturated conditions of the lateral sheaths, with $\delta_w^* \simeq 0.983$ and $T_e^* \simeq 0.967\ T_1$, and $T_1$ is the electron temperature yielding 100% of SEE; this reference temperature characterizes the SEE of the particular wall material.

The rest of equations completing Eqs. (1)-(4), their boundary conditions, their mathematical treatment, and a brief comparison with similar models [2, 3, 4] can be found in Ref. [1].

## 2 Spatial profiles and parametric investigation

Table 1 yields extensive performance data for four operational points of a thruster similar to an SPT-100 [5]. Input parameters that change for the different cases are the discharge voltage $V_d$, the magnetic strength $B_{max}$, and the SEE reference temperature $T_1$. Parameters remaining constant are listed in the table caption. Figure 1 shows the axial plasma structure for case 3. Cases 1 and 2 correspond to lower values of $V_d$, and case 4 is similar to case 3 except for the SEE properties of the walls. [Figure 2, to be discussed later, shows a more complete picture of the evolution of the main performance parameters with the discharge voltage.]

Although the profile of the magnetic field is the same in the four cases, the magnetic strength, $B_{max}$, has been adjusted in each case to the approximate point of optimum operation, this one characterized by a solution with high efficiency and fully stationary (i.e. with zero temporal oscillations). Also, the lack of satisfactory enough theories to define functional expressions for $\alpha_{ano}$ and $\nu_w$, decided us to take them as input (and constant) parameters. Part of the parametric investigation has consisting in determining their value range for the solutions of the model to recover reasonably the experimental data. This range is found to be narrow. The agreement of the results of Table 1 with experimental data, regarding both the axial plasma structure and the performance parameters, proves that the present formulation is basically correct.

### 2.1 Energy balance and temperature profile

The three main contributions to the total power loss, $P_{loss}$, come from ionization ($P_{ion}$), and plasma impacts at the anode ($P_{anode}$) and at the lateral walls ($P_{wall}$). Figure 3 compares the three contributions at different discharge voltages. Ionization and anode losses remain practically independent of $V_d$. Except for $V_d < 150V$, which is far from the nominal value of this thruster ($V_d = 300V$), energy losses at the walls are dominant.

Figure 1(e) shows that, for $V_d = 450V$, the external (from points P to E) heating of the reverse electron current, $I_{dr} = I_d - I_{i\infty}$, leaves the electrons at the chamber exhaust with a temperature, $T_{eE}$, larger than the temperature for charge-saturation of the two lateral sheaths, $T_e^* \simeq 38.6$eV. As a consequence, the electron gas suffers high energy losses near the chamber exhaust, which cools it rapidly as it moves inwards. Eventually, the lower electron temperature prevents charge-saturation of the sheaths, wall energy losses and Joule heating become of the same order [see Fig. 1(h)], leading to a gentler temperature decrease. Further inside the chamber, electron cooling from ionization becomes dominant and produces a second steep decrease of $T_e$.

For discharge voltages below 300V, the lateral sheaths are charge-saturated nowhere inside the chamber and both the energy balance and the internal temperature profile are different. Figure 4 shows the evolution of the maximum temperature, $T_{e,max}$, with the discharge voltage.

Three different slopes are observed in the curve $T_{e,max}(V_d)$ which correspond to different regimes of the temperature profile: For low $V_d$ (regime I), both the temperature gradients and the energy losses at the walls are mild and the maximum temperature occurs inside the chamber; for intermediate values of $V_d$ (regime II), the SEE yield is large in the acceleration region and $T_{e,max}$ tend to be placed near the exit; for large $V_d$ (regime III), the sheaths are charge-saturated near the chamber exhaust, the energy losses are very large there, and heat conduction helps to place $T_{e,max}$ outside the chamber. The parametric range of these three regimes depends on the SEE properties of the material too: Fig. 6 of Ref. [1] shows these regimes in terms of the SEE reference temperature, $T_1$, for $V_d$ constant.

The present near-plume model shows significant Joule heating there, yielding $T_{eE} \sim e\Delta\phi_{EP}/5$ (if $T_1$ is high enough and taking into account that heat conduction and convection are of the same order, generally). Experimental data shows that a significant part of the discharge voltage takes place outside the chamber (in region EP for us) but the electron population remains practically unheated there. This means that an external heat sink, not included in our model, must exist. The interaction of the magnetized electrons with the external walls of the chamber is the most plausible mechanism. The near-plume model will be improved to account for it. The lack of this external sink is the responsible of finding $T_{e,max}$ further downstream than experimental measurements.

## 2.2 Wall collisionality and anomalous diffusion

Figure 1(i) compares the four contributions to the electron axial diffusion frequency, $\nu_e$. From Eq. (3), the effective axial diffusion for electrons follows

$$\nu_e \sim \frac{B^2 I_{dr}}{m_e A_c n_e} \times \frac{L_c}{V_d}. \tag{10}$$

For typical SPT-100 experimental conditions, one finds $\nu_e \sim 5 \times 10^7 \mathrm{s}^{-1}$. It is well known that classical collisions between electrons and heavy particles cannot yield such a large value. It is a matter of controversy, however, whether the main contribution to $\nu_e$ comes from wall collisionality or from anomalous diffusion (based on weak plasma turbulence). The present model proves that wall collisionality, if based on SEE exclusively, contributes marginally to $\nu_e$. Refs. [2, 11] propose surface roughness and electron backscattering as mechanisms able to increase the wall collisionality to the level of being the main contribution to $\nu_e$. Here we opted for anomalous diffusion based on correlated plasma fluctuations. This mechanism was demonstrated experimentally by Janes and Lowder [6]. As in the original Bohm's formulation, we define a specific diffusion frequency in the form $\alpha_{ano}\omega_e$ where $\alpha_{ano}$ is the Bohm parameter. For the anomalous diffusion to dominate the diffusion process, it must be $\alpha_{ano}\omega_e \sim \nu_e$, which here means $\alpha_{ano} \sim 10^{-2}$. This value's range has received some indirect experimental support [9] and is the most widely used in models and simulations [7, 8, 10].

It is interesting to notice that there is a formal way to include anomalous diffusion in the electron momentum equations [1]. Let us assume the presence of fluctuations in the plasma magnitudes and, in particular, let us split the electric field and the plasma density on time-averaged components, $\boldsymbol{E}$ and $n_e$, and fluctuating components, $\boldsymbol{E}'$ and $n_e'$. Then, the electron diffusion equation is written as

$$\mathbf{0} \simeq -e(\boldsymbol{E}^* + \boldsymbol{v}_e \times \boldsymbol{B}) - (\nu_{en} + \nu_{ei} + \nu_{wm}) m_e \boldsymbol{v}_e, \tag{11}$$

where

$$\boldsymbol{E}^* = \boldsymbol{E} + \frac{\nabla n_e T_e}{e n_e} + \frac{< n_e' \boldsymbol{E}' >}{n_e} \tag{12}$$

is the generalized electric field, with the last term representing the average effect (per particle and unit of time) of correlated fluctuations of density and electric field. For a weakly-turbulent,

axisymmetric discharge, $E_\theta^*$ is expected to be the only correlated term of importance. Janes and Lowder suggested that component to be proportional to the axial force. Thus, in the lack of a better theory, we write

$$E_\theta^* = \frac{< en_e' E_\theta' >}{n_e} = \alpha_{ano} E_x^*, \qquad E_x^* \simeq E_x + \frac{1}{en_e}\frac{\partial n_e T_e}{\partial x}, \tag{13}$$

for certain parameter $\alpha_{ano}$. Operating conveniently with Eqs. (11) and (13), Eqs. (3) and (5) are reached.

There is a final remark of interest. Although correlated fluctuations are included in Eq.(3) as a collisional contribution in $\nu_e$, they are indeed part of the total electric force on the electron fluid and, as a consequence, a collisionless effect. Therefore, when anomalous diffusion dominates the electron axial diffusion, the electron dynamics are collisionless, and the component $\boldsymbol{v}_{\perp e}$ of the electron velocity perpendicular to $\boldsymbol{B}$ is given by the $E \times B$ drift based in the generalized electric field, $\boldsymbol{v}_{\perp e} = \boldsymbol{E}^* \times \boldsymbol{B}/B^2$.

### 2.3 Plasma recombination at the walls

Figure 1(b) shows that the ionization fraction is practically constant in the acceleration region. Physically this means that the main ionization region ends when the ion production has decreased to the level of the ion recombination at the walls. Then, these two effects compensate each other along the internal acceleration region, as Fig. 1(g) shows graphically, where $S_i = An_e\nu_i$ and $S_w = An_e\nu_w$. An interesting analytical relation can be obtained then. Setting $S_{iS} \sim S_{wS}$ one has

$$\eta_u = \frac{m_i I_{i\infty}}{e\dot{m}_A} \sim 1 - \tilde{\nu}_w \, \frac{v_{nS}}{v_{nA}} \, \frac{(\pi m_e/8m_i)^{1/2}}{h_c \sigma_{iS} n_{nA}}, \tag{14}$$

which relates linearly the inefficiency in the propellant utilization to the wall recombination parameter, $\tilde{\nu}_w$. This parametric relation is confirmed by Fig. 5, which presents the influence of $\tilde{\nu}_w$ on several plasma magnitudes. Also, Table 1 shows that cases 1 to 4, which use the same $\tilde{\nu}_w$, have practically the same $\eta_u$.

This study (and some more results presented in Ref. [1]) points clearly to 0.1-0.3 as the correct value's range for $\tilde{\nu}_w$. This brings up an important issue: these values of $\tilde{\nu}_w$ are too small to be justified easily by our present models for the radial dynamics. The free-acceleration model of Fife *et al.* [12] yields $\tilde{\nu}_w > 1$, whereas a more advanced model of the radial presheath [13], yields $\tilde{\nu}_w \sim 0.2$ if a 'radial friction' parameter, named $\tilde{\nu}_r$, is about 50. Physically this last situation corresponds to a strong inhibition of the ion radial flux by axial effects. However, in spite of the uncertainty on the value of $\tilde{\nu}_r$, we estimate that $\tilde{\nu}_r = O(1)$, which leaves $\tilde{\nu}_w \sim 1$. Therefore, radial/axial coupling on the ion dynamics does not seem to justify totally a low $\tilde{\nu}_w$.

This important issue leaded us to revise the radial model of Refs. [13, 14]. This model assumes a single Maxwellian distribution for primary electrons, total trapping of SEE, and a presheath/sheath structure. However, there seems to be a large evidence of different anisotropies on the electron distribution function (EDF); see, for instance, Meezan and Capelli [15] or the Russian review of Morozov and Savelyev [9]. The loss of primary electrons at the walls, the new electrons born by ionization and wall secondary emission, and the low radial collisionality would explain such a complicate EDF. In an attempt to evaluate progressively these effects we had considered already the case of partial trapping of the SEE [16]. We found that low trapping of the SEE prevented charge-saturation of the lateral sheaths and decreased the energy loss per recombined ion, that is parameter $\beta_e$ in Eq. (7). However, low trapping affects very weakly to $\tilde{\nu}_w$. In addition, partial trapping needs both experimental and numerical confirmation.

The next action, in progress now, consists of considering a bi-Maxwellian EDF with different temperatures for the directions parallel and transversal to the magnetic field, $T_{re}$ and $T_{\perp e}$. We have already demonstrated that most of the radial parameters, and $\nu_w$ in particular, depend on $T_{re}$ exclusively. These results are being implemented in the axial model now. For $T_{re} \ll T_{\perp e}$, the case of supposed interest here, the axial equations are characterized mainly by $T_{\perp e}$. Associating the different axial and radial dependences, it should turn out that $\tilde{\nu}_w \sim 0.2$ in Eq. (6) is be obtained for $T_{re}/T_{\perp e} \sim 0.1 - 0.2$. Thus, the prospects are positive, although $T_{re}/T_{\perp e} \sim 0.1$ is a too low value, in principle. Specific measurements of the ratio $T_{re}/T_{\perp e}$ would be important to support this theory.

### 2.4 The $V_d$-$B_{max}$ curve

Figure 2 shows the evolution of some plasma and thruster parameters when the discharge voltage varies from 50V to 700V. Leaving aside other factors close to 1, the thrust efficiency, $\eta$, is the product of the propellant utilization, $\eta_u$, and the current efficiency, $\eta_d = I_{i\infty}/I_d$. The discharge current is obtained from the current parameter $i_d = m_i I_d / e\dot{m}_A = \eta_u/\eta_d$, Fig. 2(d). The current efficiency (and the reverse electron current $I_{dr} = I_d - I_{i\infty}$) are related directly to the total energy losses, $P_{loss}$,by [1]

$$\eta_d \simeq 1 - P_{loss}/I_d V_d. \tag{15}$$

Two different regions are observed for $\eta$ in Fig. 2: below and above $V_d \sim 200V$. The high voltage region is the convenient operation range, with the thruster working at maximum (and almost constant) efficiency, and the specific impulse increasing as $I_{sp} \propto V_d^{1/2}$. Thruster performances deteriorate in the low voltage region: $\eta$ decreases significantly due to the combined effects of $\eta_u$ and $\eta_d = \eta_u/i_d$. First, the low $T_{e,max}$, Fig. 4, reduces the ionization rate and decreases $\eta_u$. Second, ionization losses, which depend weakly on $V_d$, become dominant there, increasing strongly the current inefficiency, $1 - \eta_d$.

The scaling law of $B_{max}$ with $V_d$ for optimum operation is a relevant subject of research, because of both its practical interest and the different results that have been reported. Figure 6(a) plots the slope $p = d\ln B_{max}/d\ln V_d$ of the $V_d$-$B_{max}$ curve of Fig. 2(a). Again, different behaviors are observed in the low and high voltage regions, which can justify the disparity of the reported data. The characteristic exponent $p$ tends to approach 1/2 in the high voltage region, and 1 in the low voltage range. (This last result is indeed related to $p = 5/4$, found in Ref. [17] for zero wall losses and $\eta_u \simeq 1$). These results verify approximately the parametric law

$$\sqrt{\frac{2eV_d}{m_i}} \sim \frac{1-\eta_d}{\eta_d} \frac{eB_{max}}{m_i \alpha_{ano}} L_{SP}, \tag{16}$$

which comes out from a dimensional analysis of the acceleration region. The length between the sonic point and the cathode, $L_{SP}$, is obtained from $L_{SP} = L_{AP} - L_{AS}$, with $L_{AS}$ plotted in Fig. 2(e). The relative error of the law (16) is shown in Fig. 6(b).

## 3 Conclusions

We stand out the following.

1) The shape of the electron temperature profile is governed by a complex energy balance, which involves ionization, Joule heating and wall losses. The two last phenomena are very dependent on the discharge voltage and the wall SEE parameter. Three different cases for the temperature profile have been identified. A correct formulation of the energy equation is found to be essential for a correct simulation of the discharge.

2) Wall collisionality based on primary/secondary electron exchanges is a marginal contribution to the axial electron diffusion. Fluctuation-based (or Bohm type) anomalous diffusion

can be included formally in the electron momentum equation. A Bohm parameter with a reduced value of $10^{-2}$ yields the most reasonable results.

3) The propellant utilization is directly proportional to the rate for plasma recombination at the walls. The axial model indicates that wall recombination is about 3 to 6 times lower than the values predicted by radial models based on Maxwellian electrons. A reduced radial temperature on the electron distribution function could explain the discrepancies.

4) The evolution of the thruster performance with the discharge voltage has shown two different operation regions. For the nominal and high values of $V_d$, maximum (and almost constant) thrust efficiency is found, and the interaction with the wall dominates the energy losses. The performance deteriorates for low voltages due to a lower ionization and, mainly, the increase of the relative energy loss ratio. The magnetic-strength versus discharge-voltage operation curve approaches $B_{max} \propto V_d^{1/2}$ for high voltages and $B_{max} \propto V_d$ for low ones.

## Acknowledgments

The authors want to thank Prof. Martínez-Sánchez for many fruitful discussions.

This research has been supported by the European Office for Aerospace Research and Development (Contract FA8655-02-M4080) and by the Ministerio de Ciencia y Tecnología of Spain (Project BFM 2001-2352).

## References

[1] E. Ahedo, J. Gallardo, and M. Martínez-Sánchez, submitted to Physics of Plasmas (2003). Partial version in *38th Joint Propulsion Conference, Indianapolis, IN, 2002*, paper AIAA 2002-4244.

[2] S. Barral, K. Makowski, Z. Peradzynski, N. Gascon, and M. Dudeck, *27th International Electric Propulsion Conference, Pasadena, CA, 2001*, paper IEPC 01-27.

[3] M. Keidar, I. Boyd, and I. Beilis, Physics of Plasmas **8**, 5315 (2001).

[4] S. Roy and B. Pandey, Physics of Plasmas **9**, 4052 (2002).

[5] J. Sankovic, J. Hamley, and T. Hang, *24th International Electric Propulsion Conference, Moscow, Russia, 1993*, paper IEPC 93-094.

[6] G. Janes and R. Lowder, Physics of Fluids **9**, 1115 (1966).

[7] J. M. Fife, *Hybrid-PIC Modeling and Electrostatic Probe Survey of Hall Thrusters*, PhD thesis, Massachusetts Institute of Technology, 1998.

[8] J. J. Szabo, *Fully kinetic numerical modeling of a plama thruster*, PhD thesis, Massachusetts Institute of Technology, 2001.

[9] A. Morozov and V. Savelyev, *Reviews of Plasma Physics*, volume 21, chapter 2, Kluwer Academic, New York, 2000.

[10] H. Tahara, D. Goto, T. Yasui, and T. Yoshikawa, *27th International Electric Propulsion Conference, Pasadena, CA, 2001*, paper IEPC 01-42.

[11] A. Bugrova, A. Morozov, and V.K.Kharchevnikov, Sov. J. Plasma Physics **16**, 849 (1990).

[12] J. Fife, M. Martínez-Sánchez, and J. Szabo, *33rd Joint Propulsion Conference, Seattle, WA, 1997*, paper AIAA 97-3052.

[13] E. Ahedo, Physics of Plasmas **9**, 3178 (2002).

[14] E. Ahedo, Physics of Plasmas **9**, 4340 (2002).

[15] N. Meezan and M. Capelli, in *36th Joint Propulsion Conference, Huntsville, AL, 2001*, paper AIAA 2001-3326.

[16] E. Ahedo and F. I. Parra, *38th Joint Propulsion Conference, Indianapolis, IN, 2002*, paper AIAA 2002-4106.

[17] E. Ahedo, J. Gallardo, and M. Martínez-Sánchez, Physics of Plasmas **9**, 4061 (2002).

| Case | 1 | 2 | 3 | 4 |
|---|---|---|---|---|
| $V_d$ (V) | 150.6 | 302.5 | 447.2 | 447.2 |
| $B_{max}$ (G) | 143.5 | 232.5 | 297.5 | 423 |
| $T_1$ (eV) | 39.9 | 39.9 | 39.9 | 197.5 |
| $F$ (mN) | 60 | 84.9 | 102.6 | 105.7 |
| $F_{pE}$ (mN) | 51.4 | 72.5 | 87.3 | 90.9 |
| $F_{p\infty}$ (mN) | 61.4 | 86.1 | 103.9 | 107.9 |
| $\eta$ (%) | 48.7 | 51.6 | 51.9 | 62.1 |
| $\eta_u$ (%) | 83.7 | 83.3 | 83.3 | 84.8 |
| $\eta_e$ (%) | 96.9 | 96.9 | 96.7 | 98.7 |
| $\eta_d$ (%) | 56.6 | 60 | 61.2 | 70.1 |
| $P_d$ (W) | 774 | 1461 | 2115 | 1882 |
| $P_{ion}$ (W) | 138.5 | 135.2 | 131.6 | 160 |
| $P_{wall}$ (W) | 135.8 | 376.8 | 601.1 | 306.9 |
| $P_{anode}$ (W) | 52.8 | 56.8 | 63.2 | 36.3 |

| Case | 1 | 2 | 3 | 4 |
|---|---|---|---|---|
| $I_d$ (A) | 5.14 | 4.83 | 4.73 | 4.21 |
| $I_{wall}$ (A) | 0.78 | 0.73 | 0.64 | 1.23 |
| $x_D$ (mm) | 4.5 | 2.6 | 1.8 | 4.6 |
| $x_S$ (mm) | 16.2 | 12.9 | 11.1 | 15.1 |
| $\Phi_{BA}$ (V) | - 4.3 | -4.8 | - 5.1 | - 4.4 |
| $\Phi_{DB}$ (V) | - 1.7 | - 1.9 | - 2.2 | - 1.1 |
| $\Phi_{SD}$ (V) | 12.6 | 14.3 | 15 | 25.7 |
| $\Phi_{ES}$ (V) | 72.6 | 168 | 255 | 212.1 |
| $\Phi_{PE}$ (V) | 71.4 | 126.9 | 184.5 | 214.8 |
| $T_{eB}$ (eV) | 2.84 | 3.37 | 3.97 | 1.89 |
| $T_{eS}$ (eV) | 19.2 | 21.9 | 22.5 | 46.9 |
| $T_{e,max}$ (eV) | 28.5 | 39.1 | 54.4 | 81.3 |
| $T_{iP}$ (eV) | 1.25 | 2.03 | 3.01 | 1.36 |
| $\delta_E$ ($^o$) | 22.7 | 18.6 | 17.9 | 22.3 |

**Table 1.-** From Ref.[1]. Main plasma parameters for different operation points of a thruster. Input parameters which remain constant are $L_c = 25$mm, $L_{EP} = 8.5$mm, $A_c = 40$cm$^2$, $\dot{m}_A = 4.78$mg/s, $T_{eP} = 4.4$eV, $\alpha_{ano} \sim 1.24 \times 10^{-2}$, $\tilde{\nu}_w \simeq 0.1912$.

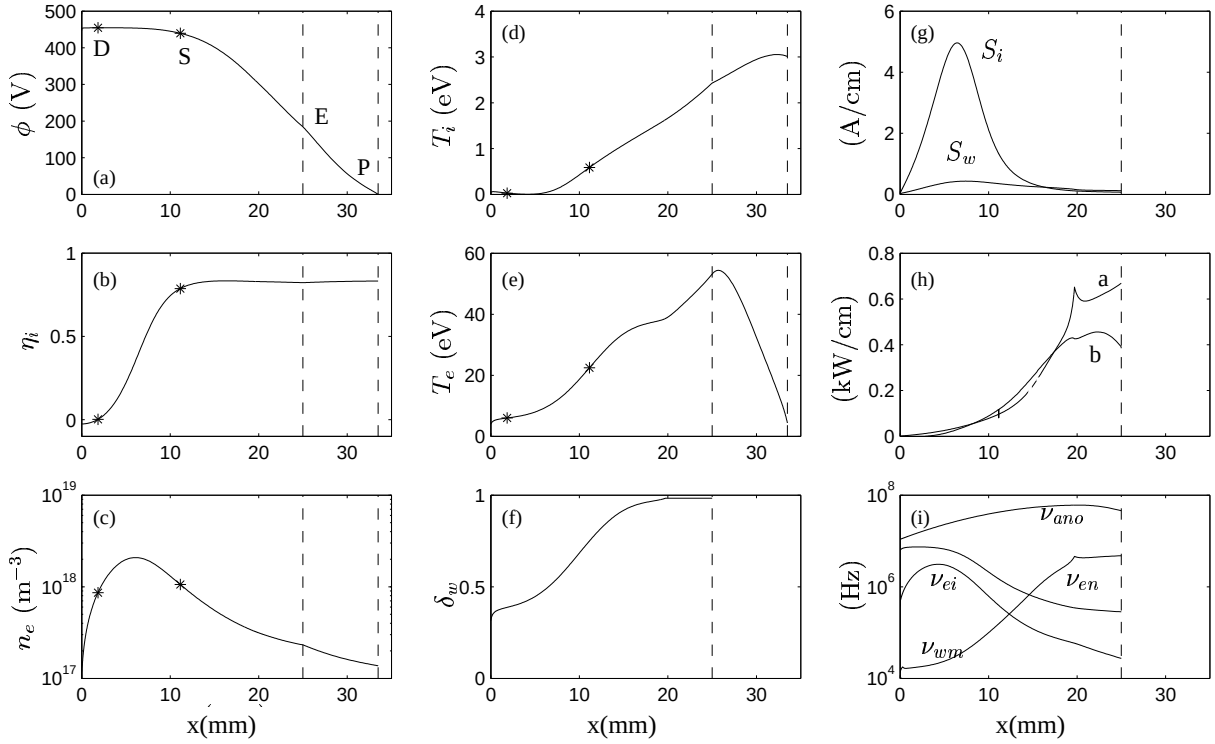


**Fig. 1.-** From Ref.[1].. Axial profiles of different plasma magnitudes for case 3 of Table 1. Asterisks represent points D and S delimiting the main ionization region; point E is the chamber exhaust and point P is the neutralization surface, the anode and the anode sheath transition (points A and B) are at $x = 0$ in the quasineutral scale. $\nu_{ano} = \alpha_{ano}\omega_e$, $S_i = An_e\nu_i$, $S_w = An_e\nu_w$. $A_c\nu_{we}n_eT_e$ and $A_cen_ev_{xe}\partial\phi/\partial x$ are 'a' and 'b', respectively, in plot (h).

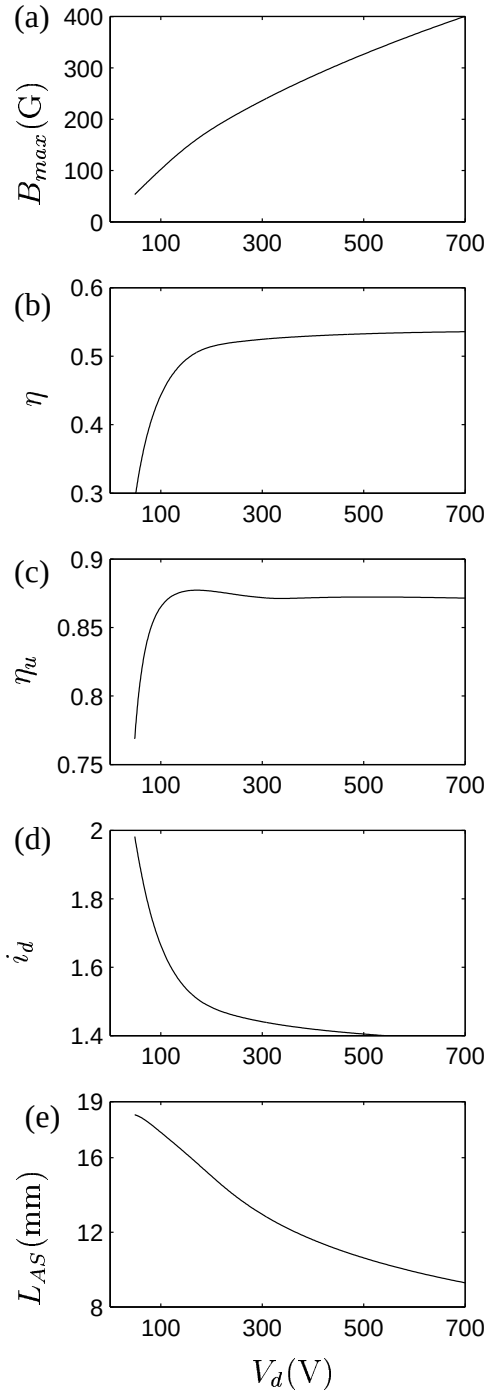


**Fig. 2.-** Evolution of the thruster performance with the discharge voltage. $B_{max}$ in subplot (a) is an input parameter, adjusted with $V_d$ to obtain an optimum solution. Other parameters are like in cases 1 to 3 in Table 1 (except for the accommodation factor for recombined ions, which here is 0.5).

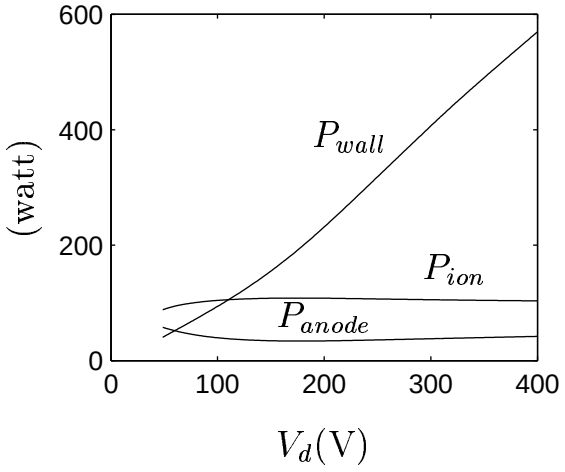


**Fig. 3.-** Main contributions to the power losses in terms of the discharge voltage for the cases of Fig. 2.

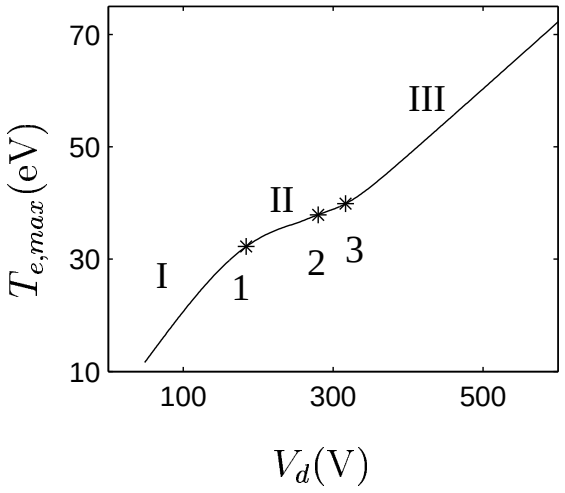


**Fig. 4.-** Maximum electron temperature in terms of the discharge voltage for the cases of Fig. 2. Points 1 to 3 correspond to $\delta_w = 0.9$, $T_{e,max} = T_{eE}$ and $T_{e,max} = T_1$, respectively. Regions I to III are defined in the main text.

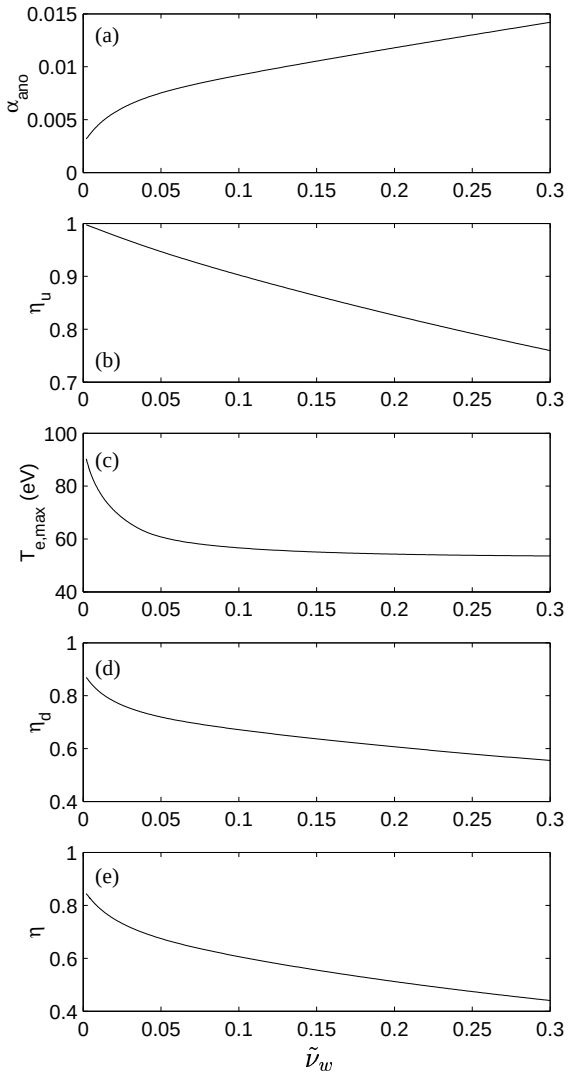


**Fig. 5.-** From Ref. [1]. Effect of the dimensionless wall-recombination frequency, $\tilde{\nu}_w$, on the thruster performance. $\alpha_{ano}$ has been adjusted with $\tilde{\nu}_w$ to obtain an optimum solution. Rest of parameters as in case 3.

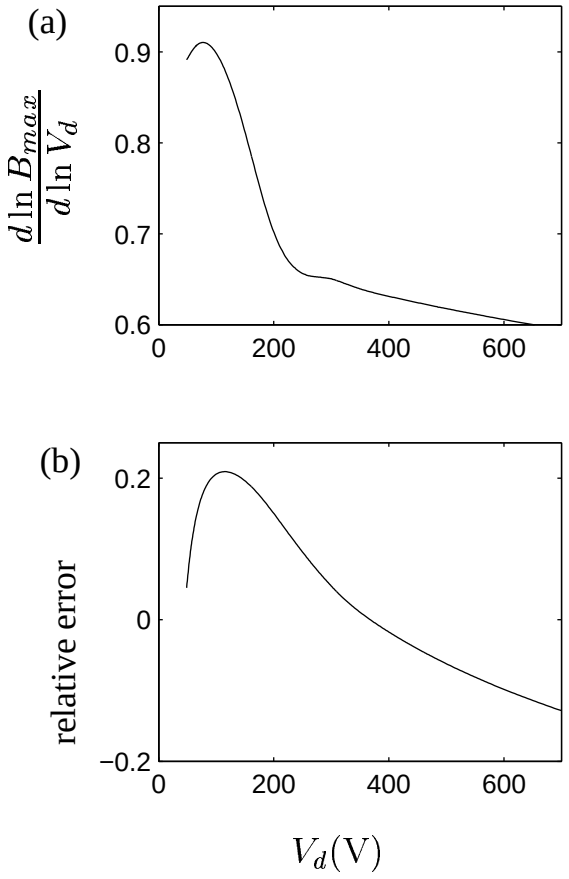


**Fig. 6.-** Evaluation of the scaling law for $B_{max}(V_d)$ for the cases of Fig. 2.